Supplementary Note 1:
Detected fluorescence vs imaging depth for through-skull 2PM and 3PM at 1320 nm

Multiphoton excited fluorescence in the mouse brain can be separated into two parts: the fluorescence within the focal volume (i.e., the signal) and the fluorescence outside the focal volume (i.e., the background). We emphasize that this background includes all fluorescence excitation away from the focal volume, not only in the axial dimension but also in the transverse dimension. The detected fluorescence is proportional to the sum of the signal and the background, while the image contrast is determined by the signal-to-background ratio (SBR). It was shown before that the in-focus signal is generated by ballistic photons, and both ballistic and scattered photons generate the out-of-focus background[1]. With increasing imaging depth, the signal decreases exponentially due to the attenuation of the ballistic photons, and the relative contribution of the background to the detected fluorescence increases. While the signal in 2PM and 3PM behave similarly with the same excitation wavelength and same mouse brain, the out-of-focus background is much more pronounced in 2PM than in 3PM, as shown in Fig. 1. In fact, for through-skull 2PM, the background contribution to the detected fluorescence is significant even at shallow depth (Fig. 1). Because the background fluorescence does not decrease rapidly with imaging depth, this leads to the apparent reduction in attenuation of the detected fluorescence for through-skull 2PM. For example, the measured effective attenuation length[2] (l_e) for through-skull 2PM (l_e=230 μm) is longer than that of 3PM (l_e=170 μm) (Fig. 1e), which is indicative of the unwanted background contribution. Indeed, the out-of-focus background in through-skull 2PM is responsible for the poor imaging contrast even at shallow depth below the skull.

The measured effective attenuation length (l_e=170 μm, Fig. 1e) in the neocortex for through-skull 3PM is much shorter than that measured with cranial windows (approximately 300 μm throughout the entire neocortex[2]). Such rapid signal attenuation can be explained by the deterioration of the PSF in through-skull imaging. As the imaging depth increases, the beam size at the skull surface also increases, which can lead to significant aberration due to the heterogeneity of the skull. As the PSF deteriorates with increasing imaging depth, less signal is generated from the focal volume and more background is produced in the wings of the PSF, even with 3PE. This is corroborated by the decline in the SBR for through-skull 3PM (Fig. 1d), which has an SBR ~ 10 at the imaging depth of ~ 500 μm. Previous work of 3PM with cranial windows achieved SBR ~ 100 at > 1000 μm imaging depth[3]. The measured effective attenuation length for through-skull imaging represents the combined effect of scattering by the brain tissue and wavefront distortion by the skull. Therefore, the effective attenuation length of the brain tissue in through-skull 3PM is much shorter than that with imaging through the cranial window.

We have neglected the dependence of fluorescence collection efficiency on imaging depth in the above analysis, which is justified because of the relatively shallow imaging depths (< 500 μm) in this study. Furthermore, the different pulse width used in 2PM and 3PM has no measurable impact on the data obtained in Fig. 1e. (see Supplementary Fig. SN1. 1).

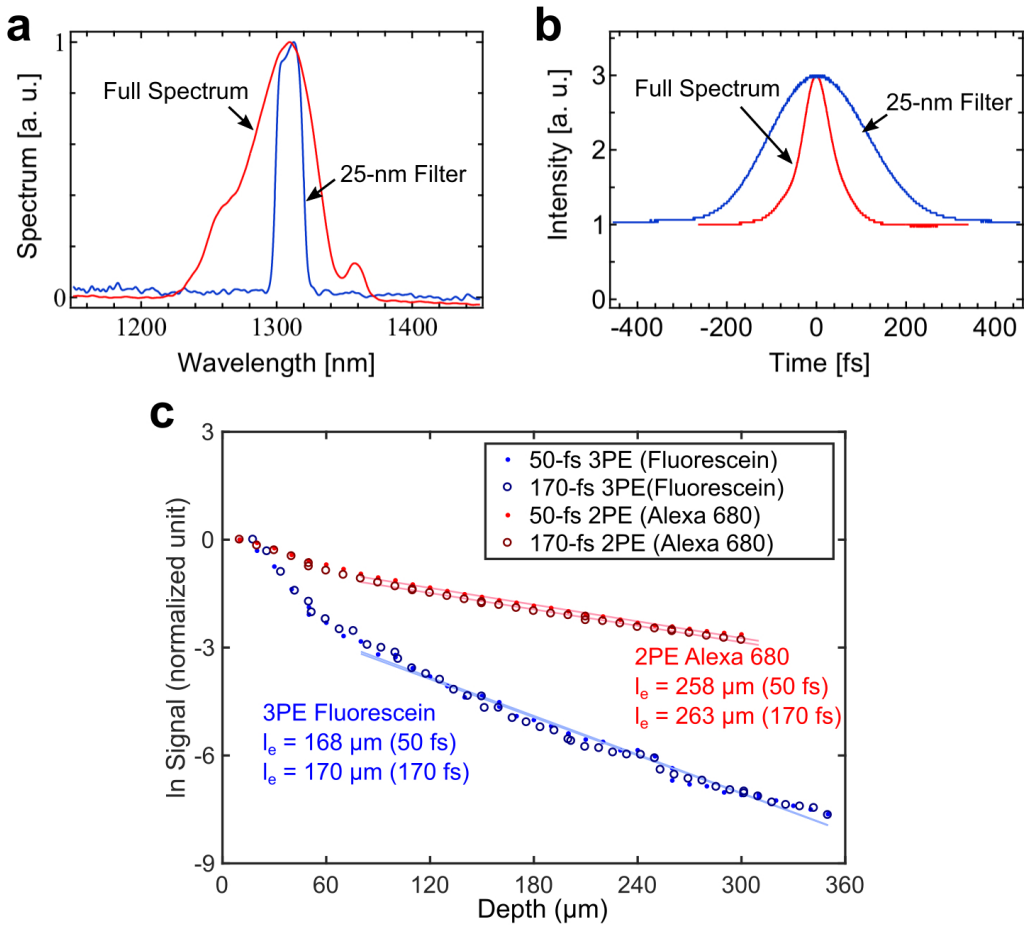

Supplementary Note 1 Figure 1 | Tissue Attenuation Length vs Excitation Pulse Duration. **a**, The full spectrum of the excitation pulses and the spectrum filtered by a 25-nm bandpass filter (a.u. means arbitrary units; n=3).
b, Intensity autocorrelation traces of the original pulses and the spectrally filtered pulses. The measurements were performed under the objective, and the pulse durations were measured to be 50 fs and 170 fs, respectively, assuming sech^2 pulse shape (a.u. means arbitrary units; n=3).
c, The effective attenuation lengths measured through an intact skull of ~120 μm thickness (n=2). The experiment setup was similar to that used for Fig. 1e, except that pulses of 50 fs and 170 fs were used to measure the attenuation lengths. The effective attenuation lengths were measured for 3PE of fluorescein and 2PE of Alexa 680. Despite the large difference in pulse duration, the difference in the effective attenuation lengths is negligible.

Supplementary Note 2:
Tissue Damage Assessment using Immunohistology and the limits of through-skull 3PM

The immunostaining results (Supplementary Fig. 6) show that 60 mW average power under the objective lens at 400 kHz repetition rate did not cause measurable damage, while 120 mW at 400 kHz repetition rate caused activation of both heat shock protein and glial fibrillary acidic protein. These results are consistent with our longitudinal studies, where neurons remained viable after hours of exposure to as high as ~ 70 mW under the objective lens at 800 kHz repetition rate. The thermal damage threshold for through-skull imaging where the skull is intact is probably lower than that for imaging through the cranial window where a significant portion of the skull is removed. As shown in one previous study, the high thermal conduction through the cranial window plays a significant role in cooling the brain surface, and the maximum temperature rise occurred at hundreds of microns below the brain surface when imaging through the cranial window[4].

No measurable nonlinear tissue damage was detected in the imaging plane (~ 200 μm below the brain surface) with 60 mW average power at 400 kHz repetition rate (Supplementary Fig. 6). The activity recordings at depths between 240 μm and 400 μm used similar average power at 800 kHz repetition rate, and had larger FOV (Fig. 2, Supplementary Figures 3 and 4). Therefore, no measurable nonlinear photodamage is expected in the focal plane under the conditions for activity imaging in this study.

The limits on FOV, temporal resolution, and imaging depth for activity recording are ultimately determined by the characteristics of the fluorescent probe, and the maximum allowable average power under the objective lens and peak power at the focus. In shot-noise-limited optical detection and assuming that the sampling rate is sufficiently high relative to the response time of the indicator, the quality of the activity recording can be quantified by the discriminability parameter[5], d', which is determined by the mean value of the baseline fluorescence photon-count rate per neuron (F_0, Supplementary Figures 3) and the characteristics of the indicator, i.e., the ΔF/F and the *1/e* decay time τ, $d' = (\Delta F/F)\sqrt{F_0\tau/2}$ (See ref. 2 for details). Using the values for GCaMP6s (ΔF/F for a single action potential ~ 30% and τ ~ 2.0 s)[6], F_0 ~ 100 photons/neuron/s is required for d'=3, which yields ~ 93% true detection and 7% false detection rate for an isolated single action potential[5]. If d' ~ 3 is used as the criteria for acceptable recording quality, our immunostaining results and chronic imaging results indicate that a 320 μm x 320 μm FOV in the cortical layer 2/3 is achievable for through-skull 3PM of GCaMP6s without measurable tissue damage. Deeper imaging is possible by reducing the repetition rate of the excitation (e.g., 400 kHz, Supplementary Figure 4c), albeit at the expense of a reduced FOV or frame rate.

References

1. Theer, P. & Denk, W. On the fundamental imaging-depth limit in two-photon microscopy. *J. Opt. Soc. Am. A* **23,** 3139–3149 (2006).
2. Kobat, D., Horton, N. G. & Xu, C. In vivo two-photon microscopy to 1.6-mm depth in mouse cortex. *J. Biomed. Opt.* **16,** 106014 (2011).
3. Horton, N. G. *et al.* In vivo three-photon microscopy of subcortical structures within an intact mouse brain. **7,** 205–209 (2013).
4. Podgorski, K. & Ranganathan, G. Brain heating induced by near infrared lasers during multi-photon microscopy. *bioRxiv* 057364 (2016). doi:10.1101/057364
5. Wilt, B. A., Fitzgerald, J. E. & Schnitzer, M. J. Photon shot noise limits on optical detection of neuronal spikes and estimation of spike timing. *Biophys. J.* **104,** 51–62 (2013).
6. Chen, T.-W. *et al.* Ultrasensitive fluorescent proteins for imaging neuronal activity. *Nature* **499,** 295–300 (2013).